


## Article

# Investigation of Thermo-Hydraulic Performances of Artificial Ribs Mounted in a Rectangular Duct

B. Varun Kumar <sup>1</sup>, P. Rajesh Kanna <sup>2</sup> , G. Manikandan <sup>1</sup> , Dawid Taler <sup>3</sup>, Jan Taler <sup>4,\*</sup>, Tomasz Sobota <sup>3</sup>   
and Marzena Nowak-Ocłoń <sup>4</sup>

<sup>1</sup> Velammal College of Engineering and Technology, Madurai 625107, India; bvarunkumar09@gmail.com (B.V.K.); gmk@vcet.ac.in (G.M.)

<sup>2</sup> CO<sub>2</sub> Research and Green Technologies Centre, Vellore Institute of Technology, Vellore 632014, India; prkanna@gmail.com

<sup>3</sup> Department of Thermal Processes, Air Protection and Waste Management, Cracow University of Technology, 31-155 Cracow, Poland; dtaler@pk.edu.pl (D.T.); tomasz.sobota@pk.edu.pl (T.S.)

<sup>4</sup> Department of Energy, Cracow University of Technology, 31-864 Cracow, Poland; marzena.nowak-oclon@pk.edu.pl

\* Correspondence: jan.taler@pk.edu.pl

**Abstract:** This research investigates the fluid flow characterization and thermohydraulic performances (THP) of rib surfaces, using computational and experimental methods. ANSYS computational fluid dynamics (CFD) software was used to predict and validate the findings in the experimental setup. Artificial rib surfaces, including polygonal and forward trapezoidal-shaped ribs, were placed in the absorber plate at different relative pitch distances ( $p/e$ ) = 6.7, 10, 13.4 and relative height ( $e/d$ ) = 20, and the mass flow rate of air (working fluid) varied at Reynolds numbers ranging from 2000 to 20,000. According to the validation results, the RNG renormalization  $k-\epsilon$  model was selected for the investigation. The results show that strong turbulence occurred closer to the wall surface and behind the rib surface, enhancing thermal performances due to the sharp edge shape of the rib. A polygonal rib with a pitch distance of  $p/e = 6.7$  achieved a higher Nusselt number (Nu) and thermo-hydraulic performance of 2.95 at Re 4000. An empirical correlation between the Nusselt number (Nu) and friction factor ( $f$ ) was developed using linear regression analysis and was compared with the predicted values. The comparison results show a close range of  $\pm 8\%$  between the experimental and predicted values.

**Keywords:** polygonal rib; forward trapezoidal rib; THP; solar air heater



**Citation:** Kumar, B.V.; Kanna, P.R.; Manikandan, G.; Taler, D.; Taler, J.; Sobota, T.; Nowak-Ocłoń, M.

Investigation of Thermo-Hydraulic Performances of Artificial Ribs Mounted in a Rectangular Duct.

*Energies* **2023**, *16*, 4404. <https://doi.org/10.3390/en16114404>

Academic Editor: Sandro Nizetic

Received: 27 April 2023

Revised: 26 May 2023

Accepted: 27 May 2023

Published: 30 May 2023



**Copyright:** © 2023 by the authors. Licensee MDPI, Basel, Switzerland. This article is an open access article distributed under the terms and conditions of the Creative Commons Attribution (CC BY) license (<https://creativecommons.org/licenses/by/4.0/>).

## 1. Introduction

The availability of solar energy is abundant in nature and can be used for drying agro-based food products such as moringa leaf, dhal, banana, etc, to convert value addition products by removing moisture levels. A solar air heater (SAH) compact device (space heating) plays a significant role in removing moisture content and is suitable for drying vegetables, fruits, grains, etc. Traditional SAH models receive heat energy directly from solar radiation and produce minimum thermal performances inside the rectangular duct. Many researchers have conducted investigations via numerical and experimental methods to augment heat efficiency. Implementing artificial rib surfaces, such as ribs, grooves, etc in the absorber plate of the SAH can produce an enhancement of the heat transfer rate. Saha et al. [1] and Kim et al. [2] conducted an experimental study on a rectangular duct with ribbed walls to investigate the heat transfer and friction characteristics of artificial rib turbulators [1] and perforated ribs [2]. The results showed that using perforated ribs and turbulators increased heat transfer by 18% and pressure drop by 12% in comparison with the smooth surface. The thermal performances of longitudinal rib turbulators were numerically investigated by Kefayati et al. [3], twisted tape inserts by Ji et al. [4], and

discrete multiple V-ribs by Balakrishnan and Khader [5]. The results indicated that the Nusselt number increased by 21% and there was a significant pressure drop compared with a smooth surface at a higher Reynolds number. Narayanan and Bhaskaran [6] and Li et al. [7] conducted their research numerically, using turbulent flow for augmentation of heat transfer in a rectangular duct with multiple ribs of varying geometry [6] and staggered saw tooth ribs [7]. They reported that using multiple ribs in the absorber plate increased heat transfer in comparison with other models and produced nominal pressure drop owing to optimum rib spacing.

Numerical simulation was carried out to investigate heat transfer and flow characteristics a rectangular duct's, for elliptical dimples rib by Wen et al. [8] and multiple dimple-shaped ribs by Wang et al. [9] The results showed that the use of multiple elliptical dimples significantly enhanced heat transfer and pressure drop compared with single elliptical dimples. Rajendra Karwa et al. [10] conducted an experimental investigation using integral chamfered ribs. The research results revealed enhancement of maximum thermal efficiency by 10% to 40%.

Ahmed et al. [11] and Sahiti and Cao [12] conducted both experimental and numerical investigations of the augmentation of heat transfer rate in a rectangular duct using wavy and perforated ribs [11] and serrated twisted tape [12]. The results showed that the use of wavy and perforated ribs increased heat transfer compared with others and pressure drop of 14% was attained. Siddiqui and Kim [13] performed experimental and numerical investigation of flow and heat transfer in a rectangular duct by using multiple V-shaped ribs. They reported that V-shaped ribs significantly increased heat transfer and pressure drop compared with a smooth surface and produced higher thermal performances. Islam and Alim [14] presented a numerical study on the thermal-hydraulic (THP) characteristics of turbulent flow in a rectangular duct with novel converging/diverging rib arrangements. The results showed that the use of these rib arrangements significantly enhanced heat transfer and pressure drop, and the optimum rib geometry was identified. Lee and Kang [15] and Seo and Kim [16] investigated the heat transfer and fluid flow characteristics in a rectangular duct with a multi-vortex generator and novel compound turbulator. The study showed that the multi-vortex generator significantly enhanced heat transfer and pressure drop, and the optimum rib geometry was identified. Karthikeyan and Kannan [17] presented a numerical study of fluid flow and heat transfer in a rectangular duct with a discrete vortex generator. The results showed that the use of the vortex generator significantly enhanced heat transfer and pressure drop, and the optimum vortex generator spacing was identified. Furthermore, various rib shapes such as transverse wire ribs [18], arc-shaped wire ribs [19], inverted U-shape ribs [20], dimple-shaped ribs [21], and W-shaped ribs [22] have been positioned in the absorber plate to augment THP by varying pitch distance, rib height, and attack angles. It was observed that higher THP values ranged between 1.72 to 1.85 and attack angle  $90^\circ$  yielded a better heat transfer rate than other angles.

From the detailed literature review, we observed that implementing a rib surface in the absorber plate of SAH enhances thermal performance compared with a smooth surface. However, many studies focused only single side inclination in rib surface, and comparison between numerical and experimental study was limited. Moreover, implementing a Sharpe edge on both sides of the rib surface produces a higher heat transfer rate closer to the wall surface. In this study, we attempted to implement a proven polygonal rib surface [23–25] in an absorber plate at various pitch distances, to identify the maximum convective heat transfer rate and THP from the rib at various mass flow rates, both numerically and experimentally.

## 2. Experimental Procedure

The experimental setup for the SAH is presented in schematic form in Figure 1. The setup consists of several main components, including:

- (i) a rectangular duct divided into three sections,
- (ii) a heating plate,

- (iii) digital thermocouples,
- (iv) a U-tube manometer,
- (v) an inclined manometer.

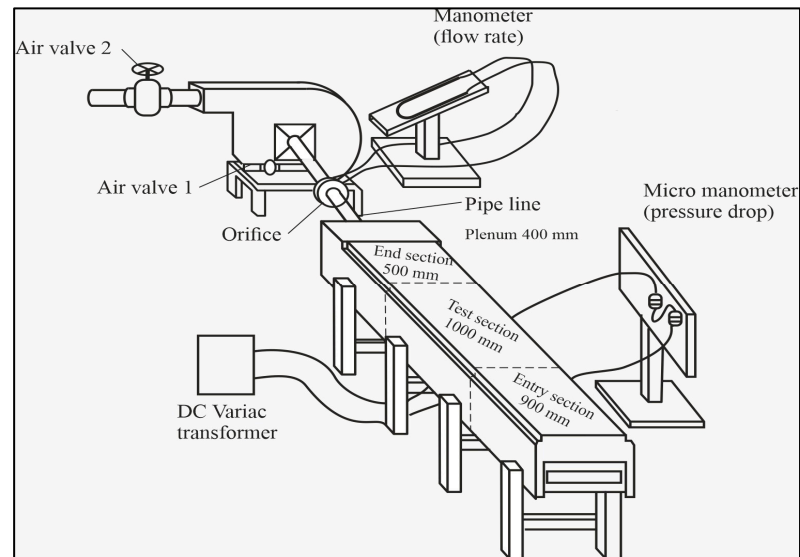


**Figure 1.** Schematic diagram of Solar Air Heater (SAH) [24].

Based on the Reynolds number, a centrifugal blower with a control valve regulates the mass flow rate/airflow through the connecting pipes. The entire rectangular duct is covered with insulating materials to prevent heat loss.

### 2.1. Test Section

The cross-sectional measurement for a rectangular wooden duct is 300 mm in width and 25 mm in height, and its entire length ( $L$ ) is 2390 mm (H). The aspect ratio ( $W/H$ ) was maintained at 12. Figure 2 shows the schematic views of the SAH and rib shapes [25] that were taken for the study. Rectangular duct lengths are (i) 890 mm for the entry portion, (ii) 500 mm for the exit section with plenum, and (iii) 1000 mm for the test section. As per the ASHRAE guidelines [26], the rectangular duct with entry and exit sections has been designed for the entry Section  $5\sqrt{WH}$  and the exit Section  $2.5\sqrt{WH}$ .

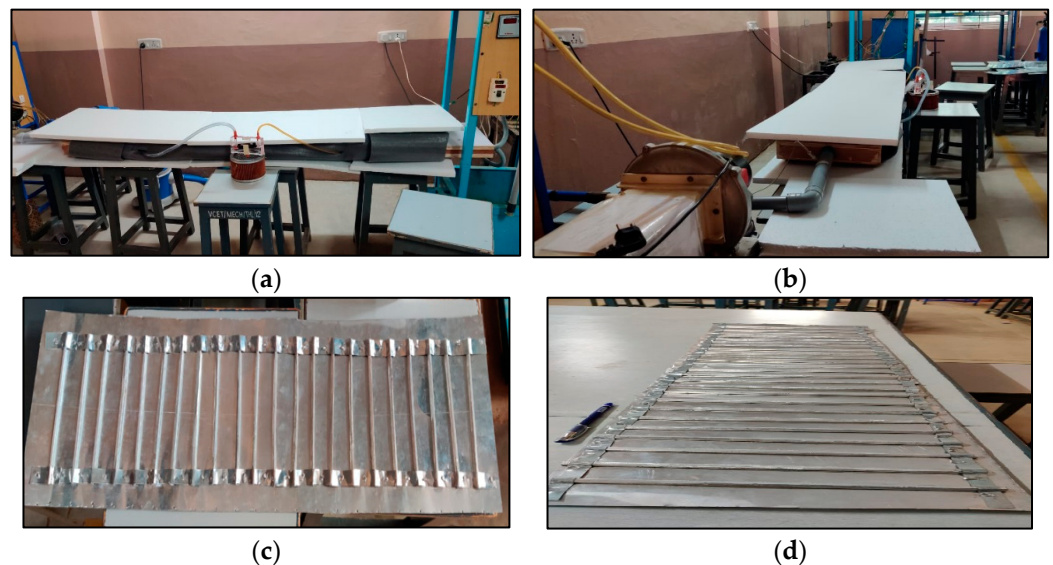


**Figure 2.** Pictorial view of the experimental setup with the rib surface [24]. (a) Side view; (b) front view and shape of rib surface; (c) top; (d) front view.

## 2.2. Absorber Plate

An aluminum sheet of 0.8 mm thickness was used as an absorber plate for the experimental research. A polygonal and trapezoidal rib with a pitch distance of 20 mm ( $p/e = 6.7$ ) was positioned. Ribs were placed one by one independently at a pitch distance of 30 mm and 40 mm ( $p/e = 10$  and  $p/e = 13.5$ ). Figure 3 illustrates the rough shapes of ribs with various pitch distances. The top surface of the absorber plate has a 6 mm thick nickel-chromium heated plate standing on it to provide heat energy equivalent to solar radiation at a constant heat flux of  $1000 \text{ W/m}^2$ .

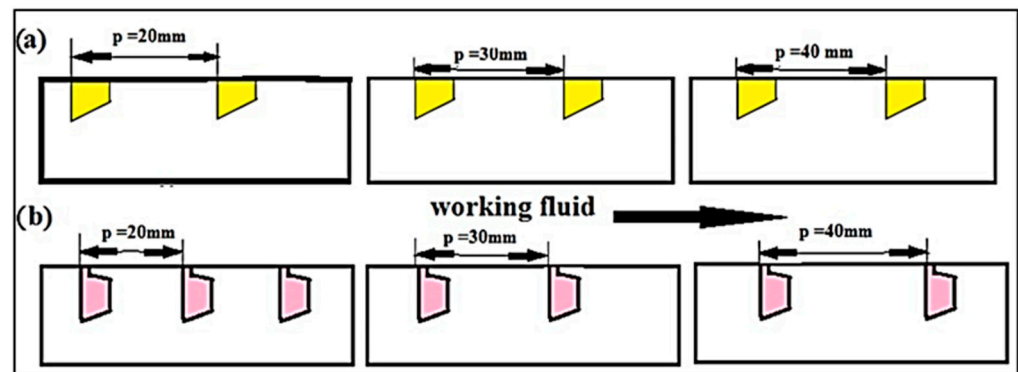


**Figure 3.** Proposed rib surfaces (a) Trapezoidal rib, (b) Polygonal rib at various pitch distances [24].

Figure 4 depicts the placement of electric resistances with 60-volt energy. A voltage regulator manages and regulates the energy supply to the heating plate. For heat protection, glass wool and thermo-form of 4 cm thickness were employed to cover the entire experimental apparatus.

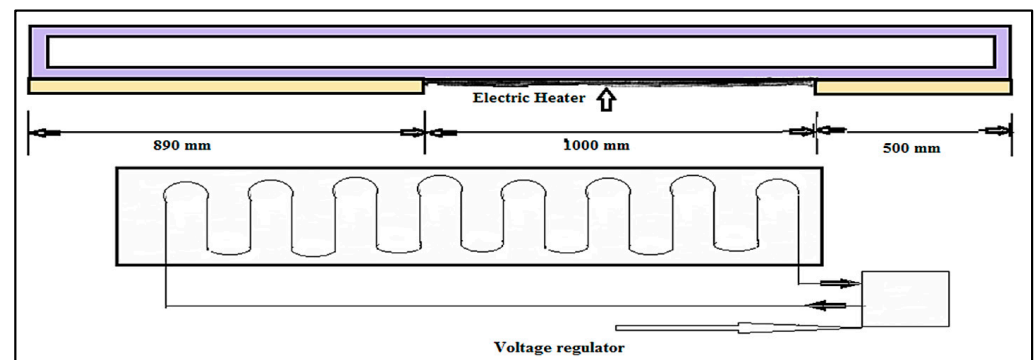


**Figure 4.** Electric heater plate position in the test section [24].

## 2.3. Measuring Instruments

The measurement of the mass flow rate and pressure drop across the orifice was conducted across the test section; pressure was measured using an inclined manometer. To ensure accuracy, butyl alcohol with a density of  $800 \text{ kg/m}^3$  was used. Sixteen thermocouples with calibrated copper constants were placed in the SAH, as illustrated in Figure 5, to measure the orifice temperature, with a U-tube manometer between the plenum and the centrifugal blower to measure the pressure drop at different locations.



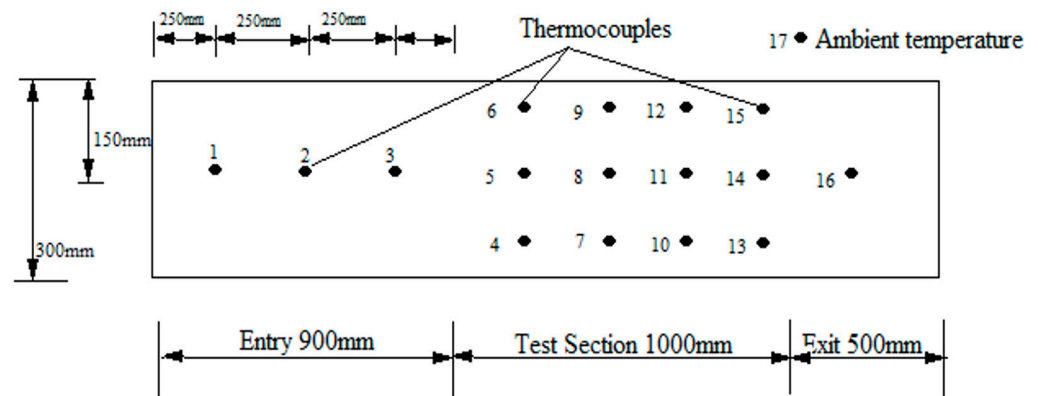


Figure 5. Location of thermocouple in absorber plate [24].

#### 2.4. Working Procedure

The experimental setup was designed according to ASHRAE guidelines [26]. To achieve steady-state conditions, the centrifugal blower was initially turned on and operated for 30 min to establish the fluid flow inside the channel. The mass flow rate was determined using a U-tube manometer at a constant velocity. All sensors were calibrated and carefully mounted to ensure accurate data collection, while the mass flow rate within the conduit was verified to remain consistent. The upper surface of the absorber plate was utilized as the heating plate, receiving a constant heat flux of  $1000 \text{ W/m}^2$ . The test section consisted of a flat absorber plate, followed by a rough plate, tested sequentially to enhance thermal performance. The data obtained were analyzed and compared on a plot in order to determine the most effective approach. Various parameters were measured in the investigative work.

- In total, 12 different temperatures recorded in the test section (tp), inlet (ti), outlet (to), and ambient temperature (ta) were measured for analysis
- Pressure drop readings were observed at the exit section of the duct ( $\Delta p$ ).
- $f$  was measured by the pressure drop across the test section ( $\Delta p_o$ ).

To record readings in the SAH's smooth and rib surface, the experiment was run constantly. The empirical equations developed by Dittus and Boelter and by Blausis were applied to validate the experimental findings for the smooth surface of Nu, and  $f$  was subsequently expanded to account for surface roughness. This led to the development of the empirical correlation for the experimental Nu and  $f$  from the regressive analysis for further research.

#### 2.5. Uncertainties Analysis

The primary measurements contained errors that contributed to the uncertainties observed in the experimental results. To conduct the uncertainty analysis, numerous methods are available ([27–29]). The analysis followed here is the methodology outlined by Holman [30]. Consider a result  $R$ , determined by a specific function involving independent variables  $X_1, X_2, X_3, \dots, X_n$ . In that result,  $R$  is the function of independent variables ( $X_1, X_2, X_3, \dots, X_n$ ), where  $R = R(X_1; X_2; X_3; \dots; X_n)$ .

The uncertainty in the result denoted as  $W_R$ , can be calculated using the equation provided by Holman [30]. Additionally,  $W_1, W_2, W_3, \dots, W_n$  represent the uncertainties associated with the independent variables  $X_1, X_2, X_3, \dots, X_n$ , respectively.

The following equation was used to calculate the values of  $W_R$ :

$$W_R = \left[ \left( W_1 \frac{\partial R}{\partial X_1} \right)^2 + \left( W_2 \frac{\partial R}{\partial X_2} \right)^2 + \dots + \left( W_n \frac{\partial R}{\partial X_n} \right)^2 + \right]^{0.5} \quad (1)$$

The relative error can be calculated using the following equation:

$$E_R = W_R / R\% \quad (2)$$

The uncertainties and relative error equations were used to evaluate the temperature difference across the heater, air mass flow rate, thermal efficiency, useful heat gained, and the convective heat transfer coefficient of the SAH. The corresponding values are provided in Table 1.

**Table 1.** Uncertainties and relative error values.

S. No	Parameter	Attained Values in SAH	Uncertainties	Relative Error (%)
1	Temperature differences (°C)	16	±0.17	0.67
2	Heat flux (W/m <sup>2</sup> )	1000	±7	0.71
3	Thermal efficiency (%)	77.9	±0.02	0.027
4	Connective heat transfer (W/m <sup>2</sup> °C)	47.9	±0.71	1.71
5	Useful heat gained by SAH (W)	872.8	±8.1	1.57

### 3. Numerical Setup

The schematic layout of the proposed experimental setup with the proposed rib surface, as depicted in Figure 6, was simulated in the computational fluid dynamics (CFD) software. The boundary conditions included an inlet section (890 mm) where air entered the rectangular duct from the left side, a test section at 1000 mm, and an exit section at 1000 mm. The 2-D schematic diagram and the proposed rib surface are illustrated in Figure 6a,b, respectively. Based on the findings from the experimental work, a sudden increase in heat transfer was observed starting from Reynolds number (Re) 5000. To simulate this phenomenon numerically, we assumed a mass flow rate range of Re 6000 to Re 20,000, encompassing the Reynolds numbers where significant heat transfer enhancements were observed in the experimental results. Thermo-physical properties of the working fluid and absorber plate are presented in Table 2. Furthermore, a grid-independent study was conducted at four different element sizes to verify Nusselt number variation. It was found that 168,314 node and element size 0.22 mm produced the least difference compared with the earlier element size 0.24 mm, as shown in Figure 7a,b. Therefore, an element size of 0.22 mm was considered for further study.

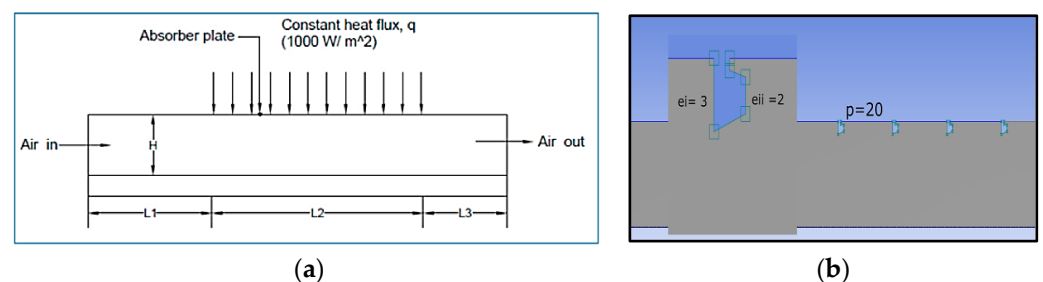


**Figure 6.** Schematic layout of the (a) rectangular duct and (b) zoomed polygonal rib at  $p = 20$  mm.

**Table 2.** Thermo-Physical Properties of Air and Absorber plate (Aluminium) for analysis [23].

S. No	Property	Air	Aluminum
1	Density, $\rho$ (kg m <sup>-3</sup> )	1.117	2719
2	Specific heat, $C_p$ (J kg <sup>-1</sup> K <sup>-1</sup> )	1007	871
3	Thermal conductivity $k$ (W m <sup>-1</sup> K <sup>-1</sup> )	0.0262	202.4
4	Viscosity $\mu$ (N m <sup>-2</sup> )	$1.857 \times 10^{-5}$	-
5	Prandl number, Pr.	0.71	-



**Figure 7.** Grid-independent study of proposed geometry at various element cells (a,b).

### 3.1. Governing Equation

The continuity, momentum, and energy equations can be utilized to express the governing equations for steady-state, two-dimensional airflow in a solar air heater with artificial roughness. These are the equations:

- i. Mass conservation or continuity equation:

$$\frac{\partial}{\partial x_i}(\rho u_i) = 0 \quad (3)$$

- ii. Momentum conservation or Navier–Stokes equation:

$$\frac{\partial}{\partial x_i}(\rho u_i u_j) = -\frac{\partial p}{\partial x_i} + \mu \frac{\partial}{\partial x_j} \left( \frac{\partial u_i}{\partial x_j} + \frac{\partial u_j}{\partial x_i} \right) \quad (4)$$

- iii. Energy conservation equation:

$$\frac{\partial(\rho u_j T)}{\partial x_i} = \frac{\partial}{\partial x_j} \left( \Gamma + \Gamma_t \frac{\partial T}{\partial x_j} \right) \quad (5)$$

Further analysis of non-dimensional flow parameters includes:

- iv. Reynolds number

$$Re = \frac{\rho u D}{\mu} \quad (6)$$

- v. Nusselt number

$$Nu = \frac{h D}{\nu} \quad (7)$$

- vi. Friction factor

$$fr = \frac{(\Delta p / l) D}{2 \rho v^2} \quad (8)$$

- vii. Thermo-hydraulic performances parameter

$$THP = \frac{(Nu_r / Nu_s)}{(f_r / f_s)^{1/3}} \quad (9)$$

An empirical equation is applied to validate the smooth surface Nusselt number by:

- viii. Dittus–Boelter equation [24]:

$$Nu = 0.023 Re^{0.8} Pr^{0.4} \quad (10)$$

ix. Blasius equation:

$$f = 0.00791 \text{ Re}^{-0.25} \quad (11)$$

### 3.2. Validation of Turbulent Model

The selection and validation of a turbulent model play crucial roles in accurately predicting the thermal coefficient augmentation for a given geometry. In order to investigate this, a literature survey was conducted. The Dittus–Boelter equation (Equation 10) was used for validation purposes [31,32]. For the specific case of a smooth duct in a solar air heater, the Nusselt number (Nu) was compared among various turbulent models, including:

- (a) The standard k- $\epsilon$  model,
- (b) The renormalization k- $\epsilon$  model,
- (c) The realizable k- $\epsilon$  model,
- (d) The standard k- $\omega$  model,
- (e) The SST k- $\omega$  model.

The detailed results of this comparison are presented in Figure 8. It was observed that the RNG renormalization k- $\epsilon$  model significantly disrupted the streamline flow and provided Nusselt number values closer to those predicted by the empirical equation. In contrast, the other models either overestimated or underestimated the Nusselt number. As a result, for simulating heat transfer in the current study, the RNG renormalization k- $\epsilon$  model was selected, in agreement with reference [23]. In addition, Figure 8 shows a new form of the correlation formula for the Nusselt number Nu, taking into account 3 different ranges of the Prandtl number Pr [33].

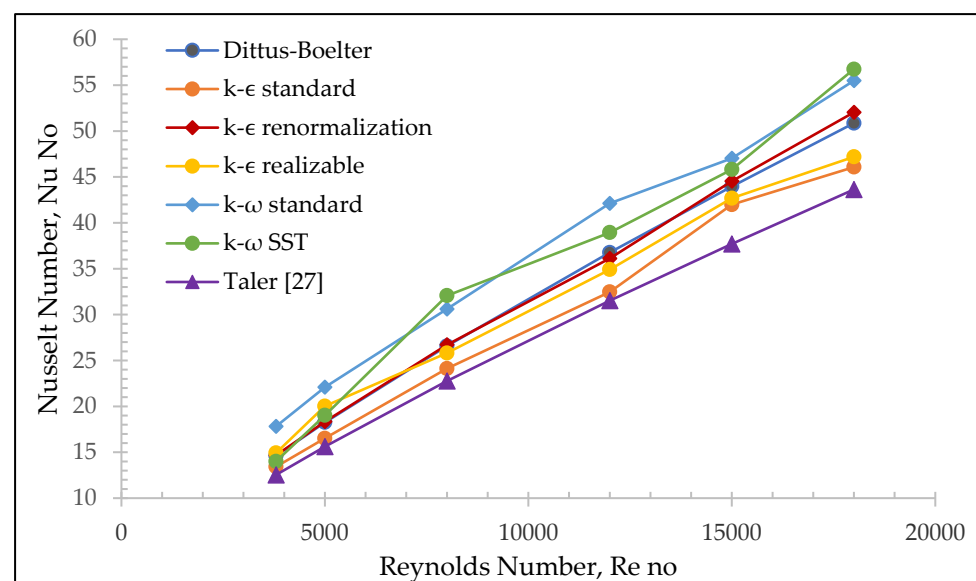


**Figure 8.** Comparison of Nu for a turbulent model with empirical Equation (8).

### 3.3. Solution Procedure

The current simulation solved the governing equations of continuity, momentum, and energy using ANSYS-Fluent version 13.0. The geometry of suggested artificial roughness, grid generation study, and solution convergent process was completed in this portion. From the model validation, the RNG renormalization k- $\epsilon$  model was selected for the numerical analysis. The SIMPLE (semi-implicit methods for pressure linked equation) pressure–velocity model was chosen with a second-order upwind discretization scheme. To achieve better results, a residual monitor was fixed at  $10^{-6}$  in the x, y, T-k model. A standard initialization was carried out in all zones. Finally, a convergent calculation was activated individually for all geometry to identify flow characterization and friction factors.

When the solution convergence was completed, an average Nusselt number and average friction factor were calculated from the results.

## 4. Result and Discussion

### 4.1. Experimental Results

Figure 9 shows the Nusselt number and friction factor values from an experimental investigation of a smooth surface absorber plate, compared to the Dittus–Boelter and Blasius empirical equations (Equations (8) and (9)) for varying Reynolds numbers. The results of the surface-averaged heat transfer (SAH) analysis reveal that as the Reynolds number increases, the Nusselt number (Nu) demonstrates improved performance, indicating enhanced convective heat transfer. Conversely, the friction factor ( $f$ ) decreases with higher Reynolds numbers, implying reduced flow resistance. Notably, at a Reynolds number of 20,000, the Nusselt number was found to be higher, while the friction factor was lower, reinforcing the observed trends. Figures 9 and 10 indicate that the experimental results are in good agreement with the empirical equations, providing confidence in the validity of the research and the possibility of further modification.

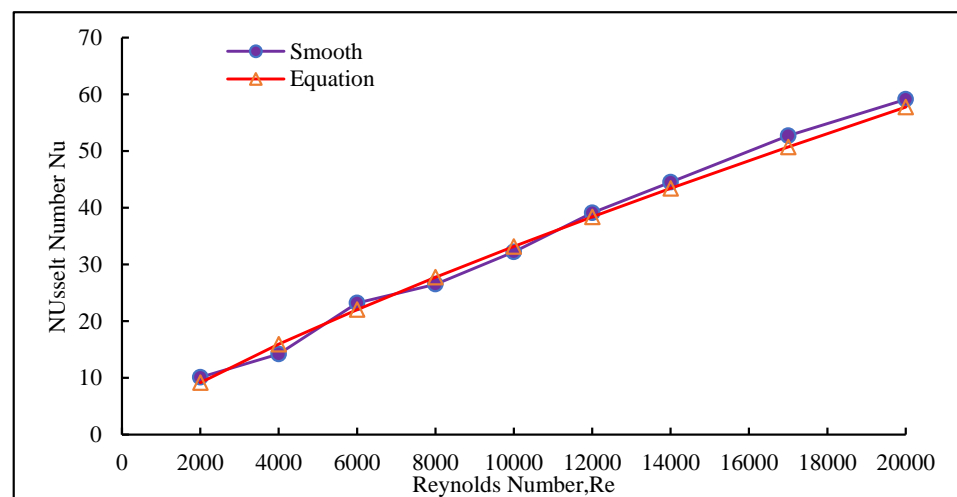


Figure 9. Comparison of experimental values with a Dittus–Boelter equation (Nu vs. Re) [24].

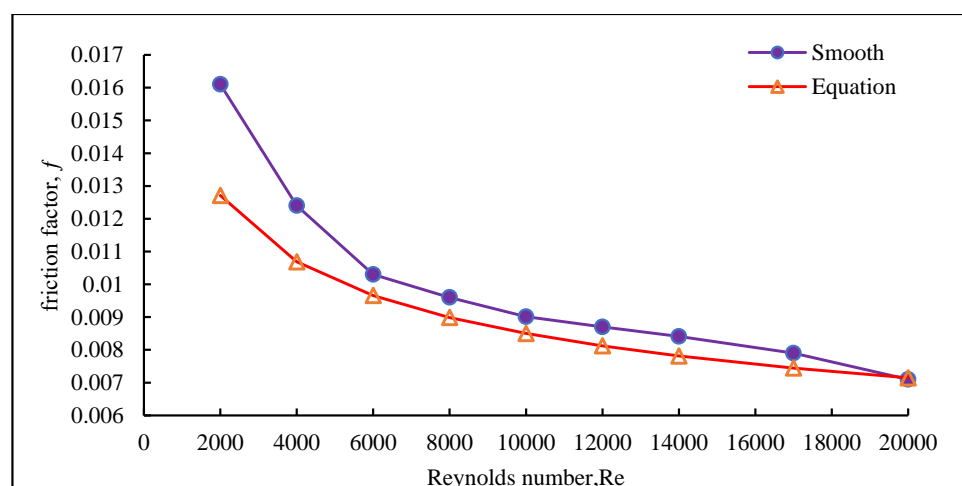


Figure 10. Comparison of experimental values with a Blasius equation ( $f$  vs. Re) [24].

#### 4.1.1. Nusselt Number Characterization

The performance of the Nusselt number (Nu) for different relative pitch distances of polygonal rib, forward trapezoidal rib, and smooth absorber plates is presented in Table 3, revealing that the Nusselt number increased with an increased Reynolds number. The



implemented rib surfaces attained a higher Nusselt number than the smooth surface, as shown in Figure 11. It is evident that incorporating a rib surface in the solar air heater (SAH) improves the heat transfer coefficient. The study suggests that implementing polygonal ribs at some relative pitch distances ( $p/e$ ) can enhance heat transfer and improve the SAH's efficiency more than others. Among them, the polygonal rib shape at a relative pitch distance ( $p/e$ ) = 10 ( $p = 30$  mm) provides the highest heat transfer rate due to the presence of sharp edges and an inclination on both sides of the rib, inducing significant turbulence in the fluid flow direction at appropriate pitch distances.

**Table 3.** Experimental values of Nusselt number vs. Reynolds number.

S. No	Re No	Smooth	Polygonal $p/e = 6.7$	Polygonal $p/e = 10$	Polygonal $p/e = 13.4$	Trapezoidal $p/e = 6.7$	Trapezoidal $p/e = 10$	Trapezoidal $p/e = 13.4$
1	2000	10.1	16.1	20.5	19.2	15.2	18.5	17.9
2	4000	14.2	38.4	48.2	46	36.7	47.5	45.9
3	6000	23.2	60.7	70.8	69	57.6	68.1	67
4	8000	26.5	70.9	80.1	79.4	67.1	77.6	75.7
5	10,000	32.2	76.9	86.4	85	70.8	81.6	80.2
6	12,000	39.1	88.9	98.6	97.8	85.5	95.7	94.2
7	14,000	44.5	107.2	117.5	115	103.2	113.9	112.5
8	17,000	52.7	115.0	125.9	123.5	109.7	120.1	119
9	20,000	59.1	134.5	145.8	144.1	124.1	139.9	137

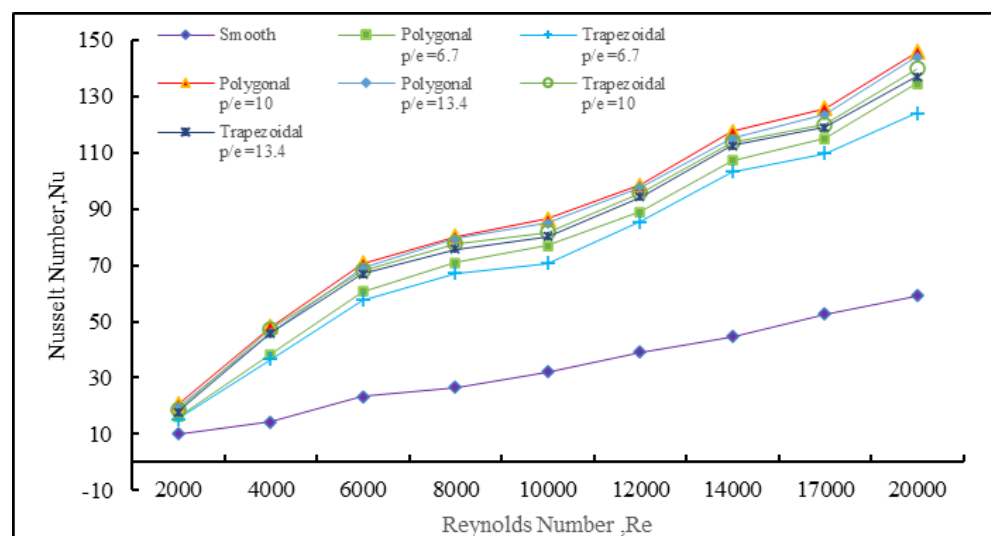


**Figure 11.** Nusselt number vs. Reynolds number for smooth and proposed roughness shapes.

#### 4.1.2. Friction Factor Characterization

In the study, Figure 12 illustrates the evaluation of friction factor for smooth and postulated surfaces (referring to the polygonal rib plate). It can be observed that the friction factor on the trapezoidal rib plate  $p/e = 13.4$  is lower than that of the other surface at higher Reynolds numbers  $Re = 20,000$ . This phenomenon can be attributed to the larger shear stresses occurring closer to the wall surface on the ribbed surface, which results in a greater pressure drop in the fluid flow direction. These findings suggest that incorporating trapezoidal rib plates can be advantageous in reducing the friction factor and slightly enhancing the system's overall efficiency compared with the polygonal ribbed surface. The detailed findings are presented in Table 4.

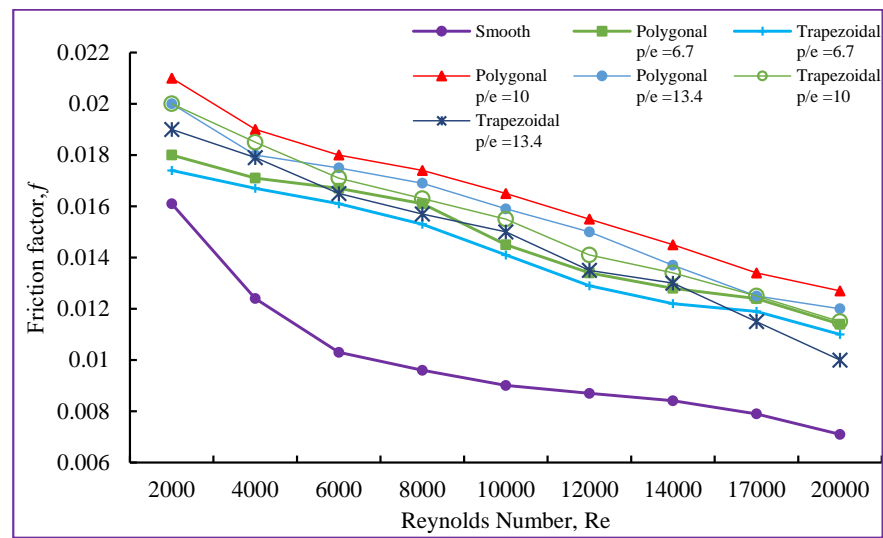


Figure 12. Friction factor vs. Reynolds number for smooth shape and proposed roughness.

Table 4. Experimental values of friction factor vs. Reynolds number.

S. No	Re No	Smooth	Polygonal p/e = 6.7	Polygonal p/e = 10	Polygonal p/e = 13.4	Trapezoidal p/e = 6.7	Trapezoidal p/e = 10	Trapezoidal p/e = 13.4
1	2000	0.0161	0.018	0.021	0.02	0.0174	0.02	0.019
2	4000	0.0124	0.0171	0.019	0.018	0.0167	0.0185	0.0179
3	6000	0.0103	0.0167	0.018	0.0175	0.0161	0.0171	0.0165
4	8000	0.0096	0.0161	0.0174	0.0169	0.0153	0.0163	0.0157
5	10,000	0.00901	0.0145	0.0165	0.0159	0.0141	0.0155	0.015
6	12,000	0.0087	0.0134	0.0155	0.015	0.0129	0.0141	0.0135
7	14,000	0.00841	0.0128	0.0145	0.0137	0.0122	0.0134	0.013
8	17,000	0.0079	0.0124	0.0134	0.0125	0.0119	0.0125	0.0115
9	20,000	0.0071	0.0114	0.0127	0.012	0.011	0.0115	<b>0.01</b>

#### 4.1.3. Thermo Hydraulic Performance (THP)

The study compared the thermal and hydraulic performance (THP) of a rib surface with a smooth surface in a solar air heater. In the experimental investigation, the researchers were interested in understanding how the proposed surface roughness affects the heat transfer and pressure drop in the SAH compared with the smooth surface. Equation (7) was used to calculate the THP of the SAH, which is an essential factor in evaluating its effectiveness and optimizing its design. The analysis report is presented in Figure 13. It reveals that using polygonal ribs with  $p/e = 10$  at Reynolds number  $Re = 4000$  resulted in THP that was 2.95 times greater than that of a smooth surface. The detailed findings are presented in Table 5. The use of polygonal ribs with a certain  $p/e$  ratio can be an effective way to enhance the performance of solar air heaters and improve their efficiency.

Table 5. Thermo hydraulic performances of proposed ribs.

S. No	Shape	p/e	2000	4000	6000	8000	10,000	12,000	14,000	17,000	20,000
1	Polygonal	6.7	1.54	2.43	2.23	2.26	2.04	1.97	2.10	1.88	1.95
2		10	1.86	<b>2.95</b>	2.54	2.48	2.20	2.08	2.21	2.01	2.04
3		13.4	1.77	2.86	2.50	2.49	2.19	2.09	2.20	2.01	2.05
4	Trapezoidal	6.7	1.47	2.34	2.14	2.17	1.90	1.92	2.05	1.82	1.82
5		10	1.71	2.93	2.48	2.46	2.12	2.09	2.19	1.96	2.02
6		13.4	1.68	2.86	2.47	2.43	2.11	2.08	2.19	1.99	2.07

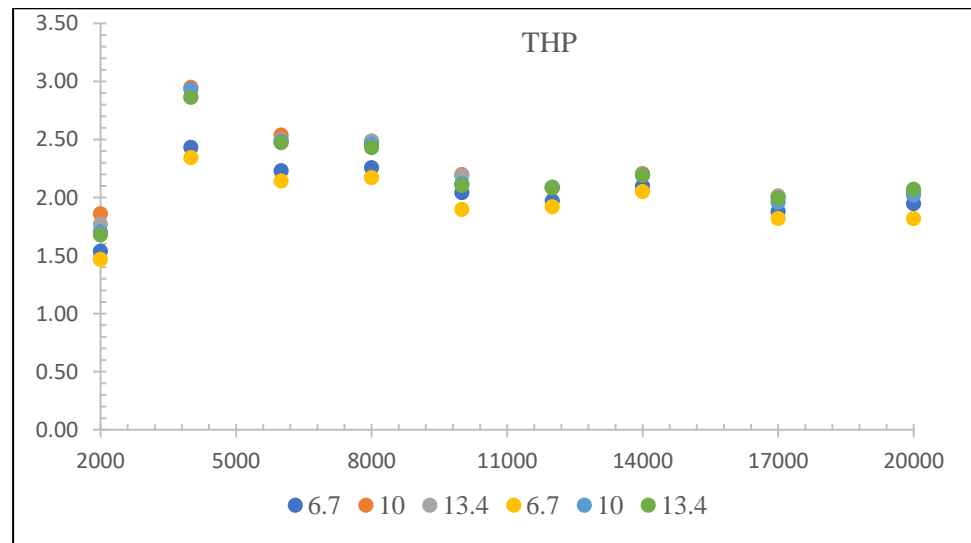


Figure 13. Thermo hydraulic performances of proposed ribs with various Reynolds numbers.

4.2. Numerical Results

4.2.1. Nusselt Number

Figure 14 illustrates the heat transfer and fluid flow characteristics of a polygonal rib surface at various pitch distances and Reynolds numbers. The results indicate that lower Reynolds numbers produced lower Nusselt numbers, whereas higher Reynolds numbers produced higher Nusselt numbers for both experimental and numerical procedures. The experimental study showed lower Nusselt numbers at  $p/e = 6.7$  ( $p = 20$  mm) and  $p/e = 13.4$  ( $p = 40$  mm) for  $Re = 6000$ , and maximum Nusselt numbers at  $p/e = 10$  ( $p = 30$  mm) for higher Reynolds numbers ( $Re = 20,000$ ) compared with the numerical procedure. Additionally, it was found that the minimum pitch distance of  $p/e = 6.7$  yielded a higher heat transfer rate than  $p/e = 10$  and  $p/e = 13.4$ . The velocity contour plot results in Figure 15 demonstrate the heat flow distribution at various pitch distances, where a strong vortex is generated near the first pair of ribs, followed by its distribution in the fluid flow direction. Moreover, increasing the Reynolds number leads to a larger vortex size generated inside the duct, resulting in higher heat transfer at higher Reynolds numbers and normal disturbances occurring in the fluid at lower Reynolds numbers for all pitch distances. Among them, the  $p/e = 6.7$  pitch distance produced stronger turbulence in the fluid flow than other pitch distances.

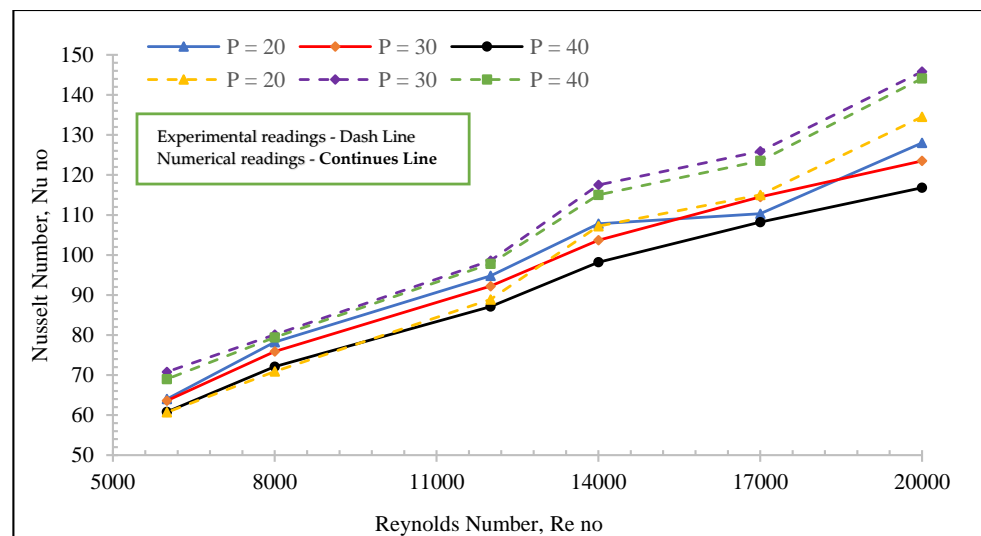
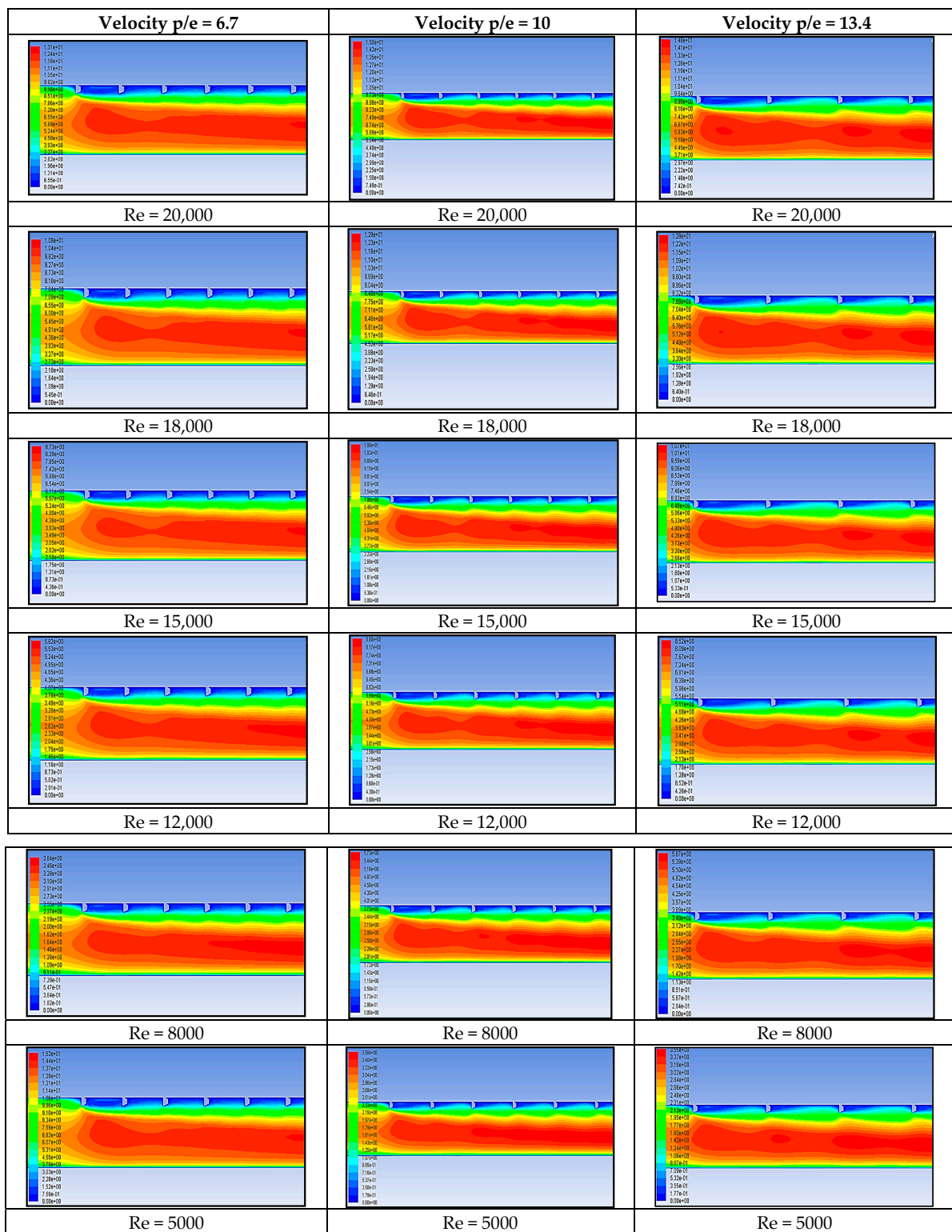


Figure 14. Numerical and experimental Nu number vs. Re number at various pitch distances.



**Figure 15.** Contour plot of velocity at various Reynolds numbers  $Re = 5000$  to  $Re = 20,000$  at  $p/e = 6.7$ ,  $p/e = 10$ ,  $p/e = 13.4$ .

The heat dissipation between rib surfaces in the fluid flow direction was investigated using a turbulent kinematic energy (T-k) model, and the results are presented in Figure 16 for all pitch distances with Reynolds numbers ranging from  $Re = 20,000$  to  $Re = 5000$ . The findings reveal that the rib surface with a closer pitch distance produced a higher heat transfer rate than the other surfaces as the Reynolds number increased. The Nusselt

number values obtained from the investigation are presented in Table 6. Furthermore, the maximum heat dissipation between the wall surface and rib surface was clearly traced in the turbulence intensity, as shown in Figure 17. It was observed that turbulence occurred from the first pair of ribs and gradually increased with each subsequent pair of ribs, and the size of the vortex also increased in the fluid flow direction. Among them, the vortex with the highest heat transfer rate at a higher Reynolds number was recorded for  $p/e = 6.4$ .

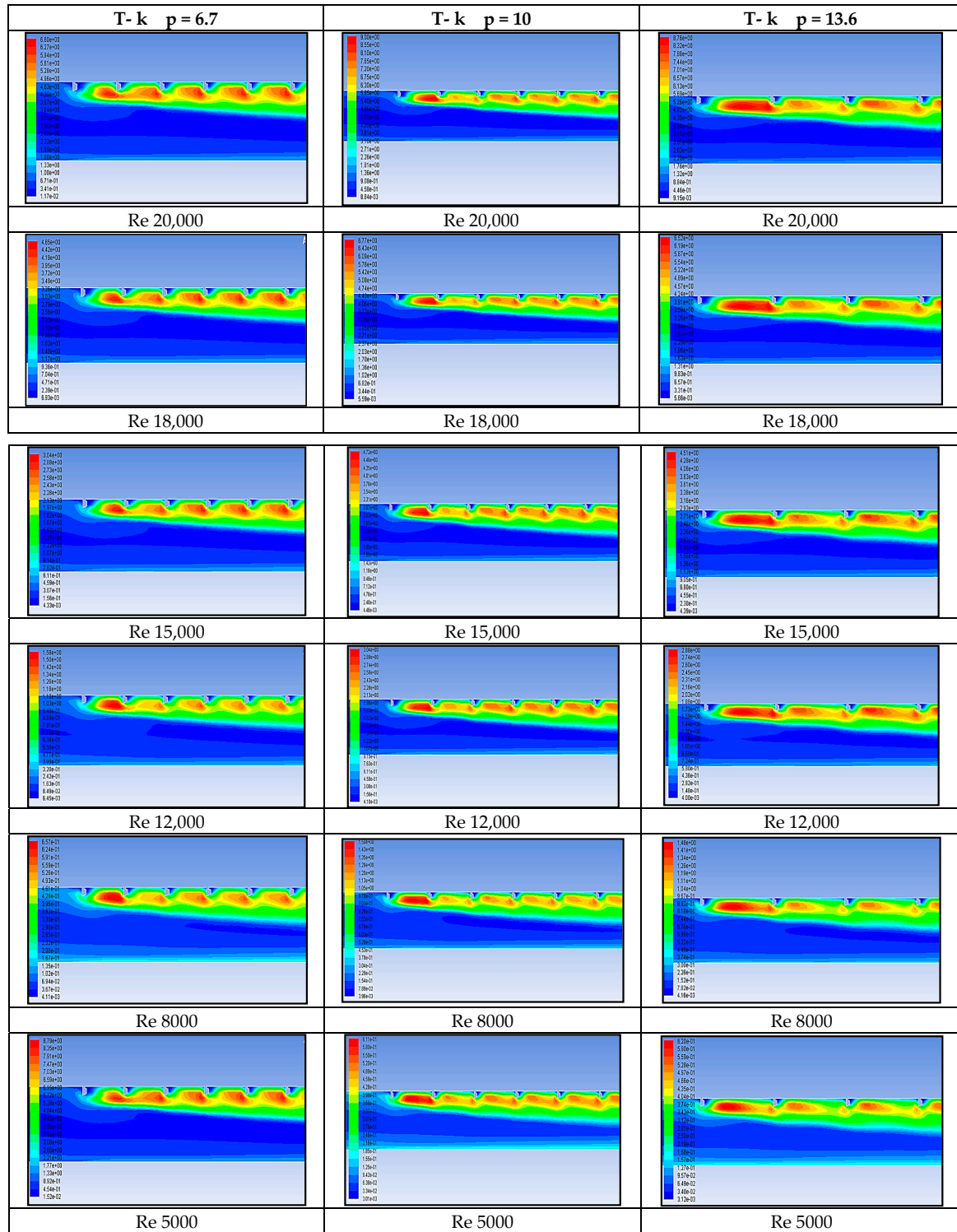


Figure 16. Contour velocity plot at various Reynolds numbers  $Re = 5000$  to  $Re = 20,000$  at  $p/e = 6.7$ ,  $p/e = 10$ ,  $p/e = 13.4$ .



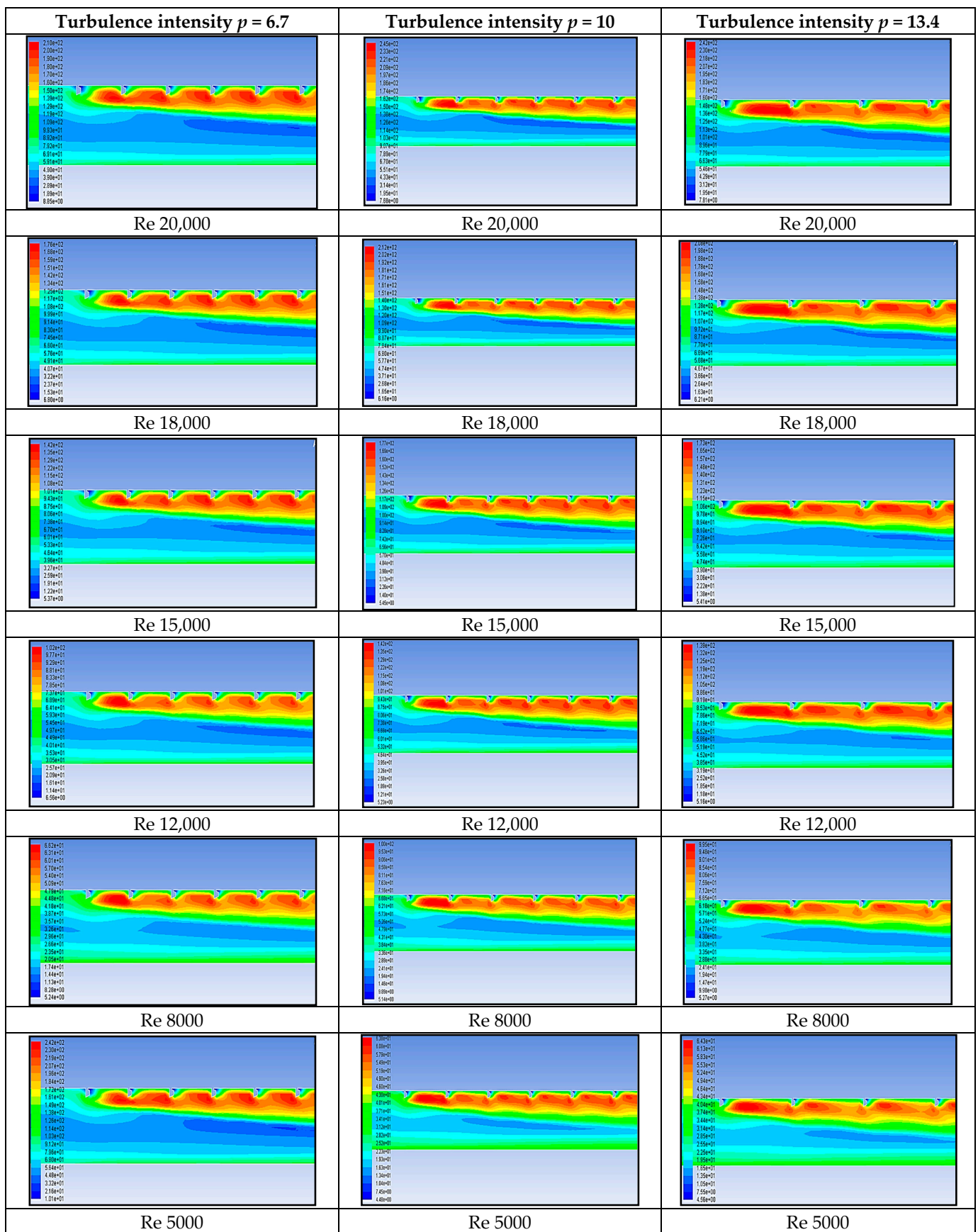


Figure 17. Contour plot of turbulence intensity at various Reynolds numbers  $Re = 5000$  to  $Re 0$  20,000 at  $p/e = 6.7$ ,  $p/e = 10$ ,  $p/e = 13.4$ .

**Table 6.** Experimental and numerical values of Nusselt number vs. Reynolds number.

S. No	Re	Numerical			Experimental		
		$p = 20$	$p = 30$	$p = 40$	$p = 20$	$p = 30$	$p = 40$
1	20,000	128	123.5	116.8	134.5	145.8	144.1
2	17,000	110.3	114.5	108.2	115	125.9	123.5
3	14,000	107.8	103.7	98.2	107.2	117.5	115
4	12,000	94.8	92.2	87.1	88.9	98.6	97.8
5	8000	78.23	75.9	72.1	70.9	80.1	79.4
6	6000	64.01	63.6	60.8	60.7	70.8	69

4.2.2. Friction Factor

The pressure drop due to the rib surface at varying Reynolds numbers was recorded in all case studies in this investigation, as shown in Figure 18. The friction factor values in relation to pitch distance and varying Reynolds numbers are presented in Table 6. It was observed that the friction factor decreased with increasing Reynolds number and increased with decreasing Reynolds number. Additionally, the experimental results produced more intense pressure drops than the numerical study. The pitch distance of  $p = 30$  mm ( $p/e = 10$ ) resulted in the highest friction losses at lower Reynolds numbers of Re 5000. The minimum pressure drops were recorded for pitch distances of  $p = 20$  mm ( $p/e = 6.7$ ) in the experimental study and  $p = 40$  mm ( $p/e = 13.7$ ) in the numerical analysis. The investigation results are summarized in Table 7, which shows that the minimum friction factor was recorded for a closer pitch distance of  $p = 20$  mm ( $p/e = 6.7$ ), owing to the higher Reynolds number causing higher heat transfer rates than the other pitch distances.

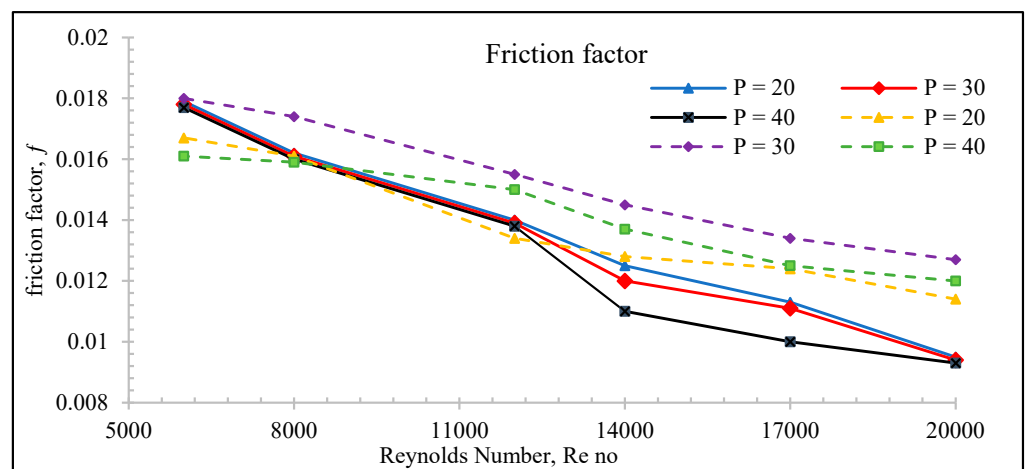


**Figure 18.** Numerical and experimental  $f$  vs. Re number at various pitch distances.

**Table 7.** Experimental and numerical values of friction factor vs. Reynolds number.

S. No	Re	Numerical			Experimental		
		$p = 20$	$p = 30$	$p = 40$	$p = 20$	$p = 30$	$p = 40$
1	20,000	0.0095	0.0094	0.0093	0.0114	0.0127	0.012
2	17,000	0.0113	0.0111	0.01	0.0124	0.0134	0.0125
3	14,000	0.0125	0.012	0.011	0.0128	0.0145	0.0137
4	12,000	0.014	0.0139	0.0138	0.0134	0.0155	0.015
5	8000	0.0162	0.0161	0.016	0.0161	0.0174	0.0159
6	6000	0.0179	0.0178	0.0177	0.0167	0.018	0.0161

The pressure drop between the polygonal rib surfaces was clearly observed and is presented in the pressure contour plot results shown in Figure 19. It was observed that at

higher Reynolds numbers, a strong vortex was generated with the closer pitch distance of  $p/e = 6.7$  for all Reynolds numbers ranging from 20,000 to 5000. Other relative pitch distances produced gradual vortices at all Reynolds numbers. It was found that lower friction occurred at relative pitch distances of  $p/e = 13.7$  in numerical investigations and  $p/e = 10$  in experimental investigations.

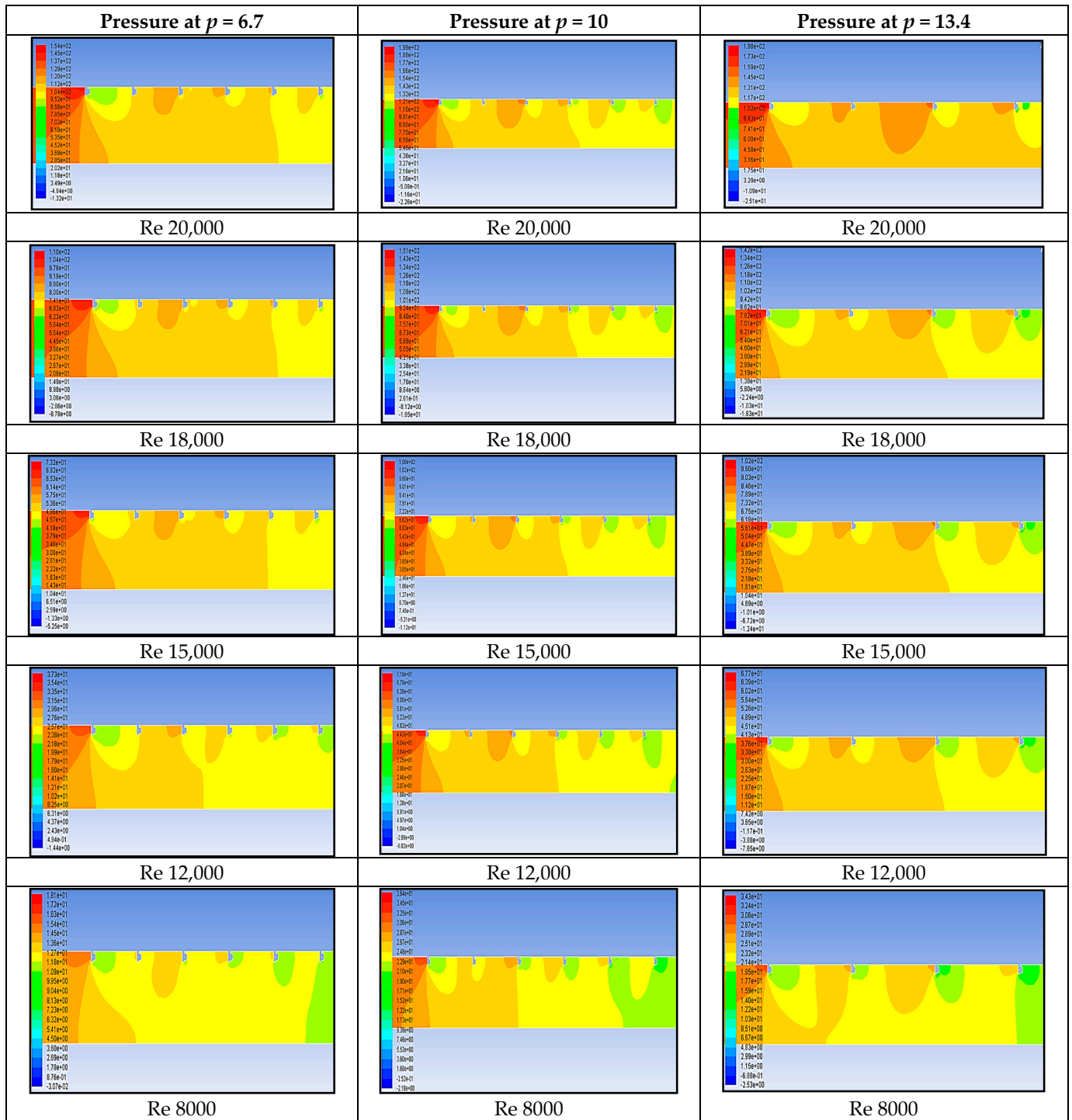
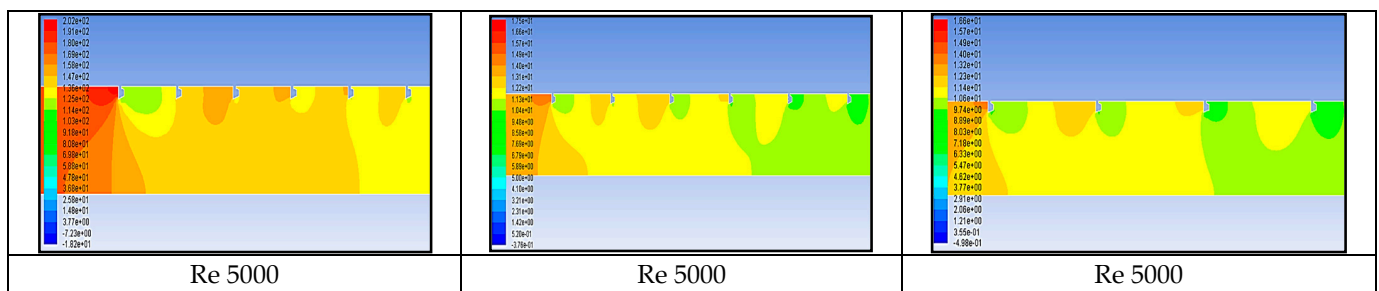


Figure 19. Cont.



**Figure 19.** Contour plot of pressure at various Reynolds numbers  $Re = 5000$  to  $Re = 20,000$  at  $p/e = 20$  mm,  $p/e = 30$  mm,  $p/e = 40$  mm.

### 5. Correlations Developed for Nusselt Number and Friction Factor

The development of an empirical correlation based on experimental investigations is important for predicting data and extending the study for further work. In this study, a correlation for the Nusselt number was developed by examining the effects of various parameters such as (a) Nusselt number increase with increasing Reynolds number,  $Re$  and (b) Nusselt number increase with relative pitch distance,  $p/e$ . Developing an accurate empirical correlation can be an essential tool for predicting the performance of the solar air heater and optimizing its design for maximum efficiency.

A second-order polynomial equation was used in straight-line regression analysis for the proposed parameters Nusselt number, Reynolds number, and relative pitch distance, and a correlation was developed [24]:

$$Nu = 0.0251 Re^{0.833} (p/e)^{0.218} \cdot \exp [0.01318 \ln (p/e)^2] \quad (12)$$

Furthermore, another correlation was developed from the observed effects of the parameters on the friction factor:

- a. Friction factor decreases with increasing Reynolds number  $Re$ .
- b. Friction factor increases with relative pitch distance,  $p/e$ .

This correlation can be used to predict the friction factor for a given combination of Reynolds number and relative pitch distance in a solar air heater. It is a valuable tool for optimizing the design and operation of the system, as it allows for the prediction of pressure drop under different conditions without the need for extensive experimentation [24].

$$f = 4.06 \cdot 10^{-6} Re^{-0.225} (p/e) \cdot \exp [-0.0117 \ln (p/e)^2] \quad (13)$$

### 6. Conclusions

The experimental and 2D numerical analysis focused on investigating the heat transfer and friction factor of polygonal and trapezoidal ribs with varying pitch distances in an SAH. The calibrated experimental and numerical results showed an enhancement of the average Nusselt number ( $Nu$ ) with an increasing Reynolds number, and a decrease in average friction factor ( $f$ ) with an increasing Reynolds number. Based on the experimental and numerical analysis, it was found that:

- a. Implementing artificial roughness in the absorber plate significantly improved the Nusselt number ( $Nu$ ) compared to a smooth surface, at all Reynolds numbers.
- b. The RNG renormalized group  $k-\epsilon$  model predicts very close results ( $\pm 3\%$ ) to the Dittus–Boelter empirical values in the numerical and experimental work.
- c. The polygonal-shaped rib, with  $p = 20$  mm (numerical) and  $p = 30$  mm (experimental), recorded the highest average Nusselt number at Reynolds number 20,000 compared with other rib shapes, indicating that it can effectively enhance heat transfer in the SAH.
- d. The minimum friction factor ( $f$ ) of 0.01 at pitch distance of  $p = 20$  in experimental work and 0.0093 at  $p = 40$  mm in numerical work was attained at Reynolds number  $Re 20,000$ .

- e. The thermo-hydraulic performance (THP) of the proposed shapes achieved the highest values of 2.95 in the polygonal rib at  $p/e = 10$  and Reynolds number 4000.
- f. An empirical correlation was developed for Nusselt number  $Nu$  and friction factor  $f$  from the experimental values in (Equation (10) and (11)), which showed maximum accuracy of  $\pm 8\%$  between experimental and calculated values.

Overall, the use of artificial roughness in SAHs can be an effective way to enhance heat transfer and improve system efficiency. The polygonal shape of the rib with  $p/e = 6.7/p = 20$  mm (numerical) and  $p/e = 10/p = 30$  mm (experimental) showed the most significant improvement in the Nusselt number, making it a promising choice for future SAH design.

**Author Contributions:** Conceptualization, methodology, investigation: B.V.K., P.R.K., Software, validation writing—review and editing: P.R.K., G.M., J.T. Formal analysis, resources, data curation: D.T., M.N.-O. Writing—original draft preparation, supervision: B.V.K., J.T., T.S. All authors have read and agreed to the published version of the manuscript.

**Funding:** This research received no external funding.

**Data Availability Statement:** Data available on request.

**Conflicts of Interest:** The authors declare that they have no known competing financial interests or personal relationships that could have appeared to influence the work reported in this paper.

## Nomenclature

A	cross-sectional area of the duct, $[A = WH]$ , $m^2$
Ac	surface area of collector plate, $m^2$
Cd	coefficient of discharge for orifice meter
Cp	specific heat of air at constant pressure, $kJ/(kg K)$
D h, d	equivalent diameter of the air passage, $[D = 4A/[2(W + H)]]$ , m
I	turbulence intensity/intensity of solar radiation, $W/m^2$
e	roughness height, mm
e/d	relative roughness height
H	height of air channel, m
h	heat transfer coefficient, $W m^{-2} K^{-1}$
k	thermal conductivity of air, $W m^{-1} K^{-1}$
L	duct length, m
L1	inlet length of duct, mm
L2	test length of duct, mm
L3	outlet length of duct, mm
m	mass flow rate of air, $kg/s$
p	roughness pitch, m
Dimensionless parameters	
f	friction factor
fr	friction factor for rough surface
fs	friction factor for a smooth surface
fexp	friction factor experimental
Nu	Nusselt number
Nus	Nusselt number for rough duct
Nur	Nusselt number for smooth duct
Nu exp	Nusselt number experimental
Pr	Prandtl number
P/e	relative roughness pitch
Re	Reynolds number
W/H	duct aspect ratio
Greek symbols	
$\mu$	dynamic viscosity, $Ns/m^2$
$\mu_t$	turbulent viscosity, $Ns/m^2$



$\rho$	density of air, kg/m <sup>3</sup>
$\alpha$	angle of attack, degree
$\varepsilon$	dissipation rate
$\omega$	specific dissipation rate
$\delta$	transition sub-layer thickness, m
$k$	turbulence kinetic energy, m
$\Gamma$	molecular thermal diffusivity
$\Gamma_t$	turbulent thermal diffusivity

## References

- Saha, S.K.; Islam, M.S.; Saha, S.K.; Alam, M.M. Experimental study of heat transfer and friction characteristics of rectangular duct with ribbed walls. *Int. J. Heat Mass Transf.* **2013**, *60*, 559–567.
- Kim, K.H.; Kim, K.Y.; Ha, M.Y. Heat transfer and pressure drop characteristics of a rectangular duct with perforated ribs. *Int. J. Heat Mass Transf.* **2014**, *71*, 283–291.
- Kefayati, G.R.; Safaei, M.R.; Esfahani, J.A. Numerical study on the heat transfer and pressure drop in a rectangular duct with longitudinal rib turbulators. *Appl. Therm. Eng.* **2018**, *138*, 621–632.
- Ji, H.; Luo, L.; Yan, X.; Zhang, B. Numerical investigation on heat transfer and fluid flow characteristics in rectangular ducts with twisted tape inserts. *Appl. Therm. Eng.* **2020**, *169*, 114919.
- Balakrishnan, A.R.; Khader, M.A. Numerical investigation of heat transfer augmentation in a rectangular duct using discrete multiple V-ribs. *Int. J. Heat Mass Transf.* **2015**, *91*, 421–430.
- Narayanan, R.; Bhaskaran, R. Numerical analysis of turbulent flow and heat transfer in a rectangular duct with multiple ribs of varying geometry. *J. Therm. Anal. Calorim.* **2019**, *137*, 431–446.
- Li, H.; Li, J.; Li, J.; Li, Q. Experimental study on turbulent heat transfer enhancement in a rectangular duct with staggered sawtooth ribs. *Exp. Therm. Fluid Sci.* **2021**, *124*, 111210.
- Wen, D.; He, Y.L.; Tang, G.H. Numerical investigation of heat transfer and flow characteristics in a rectangular duct with elliptical dimples. *Int. J. Heat Mass Transf.* **2019**, *132*, 9–19.
- Wang, W.; He, Y.L.; Tao, W.Q. Numerical investigation of heat transfer and fluid flow characteristics in a rectangular duct with multiple dimple-shaped ribs. *Int. J. Heat Mass Transf.* **2021**, *181*, 121458.
- Karwa, R.; Solanki, S.C.; Saini, J.S. Thermo-hydraulic performance of solar air heaters having integral chamfered rib roughness on absorber plates. *Energy* **2001**, *26*, 161–176. [[CrossRef](#)]
- Ahmed, A.E.; Ahmed, N.M.; Ahmed, M.S. Experimental and numerical investigation of heat transfer enhancement in a rectangular duct using wavy and perforated ribs. *J. Therm. Anal. Calorim.* **2020**, *139*, 465–483.
- Sahiti, N.; Cao, B.Y. Experimental and numerical investigation of heat transfer enhancement in a rectangular duct with a novel serrated twisted tape. *Exp. Therm. Fluid Sci.* **2017**, *81*, 77–89.
- Siddiqui, M.F.; Kim, M.H. Experimental and numerical investigation of flow and heat transfer in a rectangular duct with multiple V-shaped ribs. *Int. J. Heat Mass Transf.* **2018**, *117*, 689–702.
- Islam, M.S.; Alim, M.A. Numerical study on thermal-hydraulic characteristics of turbulent flow in a rectangular duct with novel converging/diverging rib arrangements. *Appl. Therm. Eng.* **2021**, *188*, 116680.
- Lee, H.J.; Kang, B.H. Heat transfer and fluid flow characteristics in a rectangular duct with multi-vortex generator. *Int. J. Heat Mass Transf.* **2020**, *160*, 120221.
- Seo, J.; Kim, Y. Experimental study of heat transfer and friction factor characteristics in a rectangular duct with novel compound turbulator. *Appl. Therm. Eng.* **2021**, *194*, 113098.
- Karthikeyan, K.; Kannan, S. Numerical study of fluid flow and heat transfer in a rectangular duct with discrete vortex generator. *Appl. Therm. Eng.* **2021**, *187*, 116438.
- Verma, S.; Prasad, B. Investigation for the optimal thermo-hydraulic performance of artificially roughened solar air heaters, Renewable. *Energy* **2000**, *20*, 19–36.
- Saini, R.P.; Saini, S.K. Development of correlations for Nusselt number and friction factor for solar air heater with roughened duct having arc-shaped wire as artificial roughness. *Sol. Energy* **2008**, *82*, 1118–1130. [[CrossRef](#)]
- Bopche, S.B.; Tandale, M.S. Experimental investigations on heat transfer and frictional characteristics of a turbulator roughened solar air heater duct. *Int. Commun. Heat Mass Transf.* **2009**, *52*, 2834–2848. [[CrossRef](#)]
- Saini, R.P.; Verma, J. Heat transfer and friction factor correlations for a duct having dimple shape artificial roughness for solar air heaters. *Energy* **2008**, *33*, 1277–1287. [[CrossRef](#)]
- Kumar, A.; Bhagoria, J.L.; Sarviya, R.M. Heat transfer and friction correlations for artificially roughened solar air heater duct with discrete W-shaped ribs. *Energy Conversat. Manag.* **2009**, *50*, 2106–2117. [[CrossRef](#)]
- Kumar, B.V.; Manikandan, G.; Kanna, P.R. Enhancement of heat transfer in SAH with polygonal and trapezoidal shape of the rib using CFD. *Energy* **2021**, *234*, 121154. [[CrossRef](#)]
- Kumar, B.V.; Manikandan, G.; Kanna, P.R. Performances of solar air heater using polygonal and trapezoidal rib absorber plate for augmentation of heat transfer. *Tierärztliche Praxis.* **2020**, *40*, 888–903.

25. Varun Kumar, B.; Manikandan, G.; Kanna, P.R.; Taler, D.; Taler, J.; Nowak-Oćoń, M.; Mzyk, K.; Toh, H.T. A Performance Evaluation of a Solar Air Heater Using Different Shaped Ribs Mounted on the Absorber Plate—A Review. *Energies* **2018**, *11*, 3104. [[CrossRef](#)]
26. *ASHRAE Standard 93*; Method of Testing to Determine the Thermal Performance of Solar Collectors. 30329. American Society of Heating, Refrigeration and Air Conditioning Engineers: Atlanta, GA, USA, 2003.
27. Holman, J.P. *Experimental Methods for Engineers*; Tata McGraw-Hill Publishing Company Limited: New Delhi, India, 2007.
28. Joint Committee for Guides in Metrology. JCGM 100: Evaluation of Measurement Data—Guide to the Expression of Uncertainty in Measurement; JCGM. 2008. (Also Known as GUM). Available online: [https://www.bipm.org/documents/20126/2071204/JCGM\\_100\\_2008\\_E.pdf/cb0ef43f-baa5-11cf-3f85-4dcd86f77bd6](https://www.bipm.org/documents/20126/2071204/JCGM_100_2008_E.pdf/cb0ef43f-baa5-11cf-3f85-4dcd86f77bd6) (accessed on 26 May 2023).
29. Kline, S.J.; McClintock, F.A. Policy on reporting uncertainties in experimental measurements and results. *ASME J. Heat Transf.* **2000**, *122*, 411–413.
30. Duffie, J.A.; Beckman, W.A. *Solar Engineering of Thermal Processes*; Wiley: New York, NY, USA, 1980.
31. McAdams, W.H. *Heat Transmission*; McGraw-Hil: New York, NY, USA, 1942.
32. Webb, R.L.; Eckert, E.R.G. Application of rough surface to heat exchanger design. *Int. J. Heat Mass Transf.* **1972**, *15*, 1647–1658. [[CrossRef](#)]
33. Taler, D.; Taler, J. Simple heat transfer correlations for turbulent tube flow. *E3S Web Conf.* **2017**, *13*, 02008. [[CrossRef](#)]

**Disclaimer/Publisher’s Note:** The statements, opinions and data contained in all publications are solely those of the individual author(s) and contributor(s) and not of MDPI and/or the editor(s). MDPI and/or the editor(s) disclaim responsibility for any injury to people or property resulting from any ideas, methods, instructions or products referred to in the content.